BULLETIN OF THE POLISH ACADEMY OF SCIENCES
TECHNICAL SCIENCES
Vol. 52, No. 4, 2004

Advanced technology of AIII-BV and AIII-N structures for microelectronics application

B. BORATYŃSKI, R. KORBUTOWICZ, B. PASZKIEWICZ, R. PASZKIEWICZ, D. PUCICKI, D. RADZIEWICZ, B. ŚCIANA and M. TŁACZAŁA*

Faculty of Microsystem Electronics and Photonics, Wroclaw University of Technology, 11/17 Janiszewskiego St., 50-372 Wroclaw, Poland

Abstract. In this work studies of MOVPE growth of InAlGaAs/AlGaAs/GaAs heterostructures are presented. The HRXRD and SIMS measurements indicate the high structural and optical properties as well as high uniformity of thickness and composition of InAlGaAs quantum wells. This work is the first step towards elaboration of the technology of the strained InAlGaAs/GaAs heterostructures for advanced optoelectronic devices working in the visible part of the spectrum.

The investigations of Si (n-type), Zn (p-type) δ-doped GaAs epilayers and centre Si-δ-doped $In_xGa_{1-x}As$ single quantum well (SQW) are presented. The δ-doping layer was formed by SiH_4 or DEZn introduction during the growth interruption. The electrical and optical properties of the obtained structures were examined using C–V measurement, EC–V electrochemical profiler, Raman spectroscopy (RS), photoreflectance (PR) and photocurrent (PC) spectroscopies.

Technology of thick GaN layers grown on sapphire by HVPE is very promising as a part of freestanding GaN substrates manufacturing. Further works will be focused on the optimisation of growth, separating layers from substrates and surface polishing.

The influence of the growth parameters on the properties of (Ga, Al)N/Al_2O_3 and Mg dopant incorporation was studied.

Keywords: heterostructure, delta-doping, MOVPE, HVPE, bandgap engineering, impedance spectroscopy.

1. Introduction

The development of very high speed electronic and optoelectronic devices depends on advanced III-V semiconductor materials. Their multicomponent structures which are obtained by metalorganic vapor phase epitaxy (MOVPE) technique make possible modification of the bandgap value. Additionally three-dimensional doping and delta-doping in nanoscale enhance bandgap engineering capability. Elaboration of the technology of semiconductor nanostructures requires clever and controlled manipulation of both material composition and doping process.

Research conducted at the Faculty of Microsystem Electronics and Photonics of Wroclaw University of Technology concentrate on the epitaxial growth of III-V semiconductor compounds as well as the design and fabrication of optoelectronic devices and monolithic microwave integrated circuits (MMICs).

In this paper the results of investigations of AlGaInAs multiquantum wells on GaAs substrates, delta-doping techniques and epitaxial growth of p-type GaN layers on sapphire substrates are presented. The technology of thick GaN layers which can be used as pseudo-bulk substrates is investigated.

2. MQW InAlGaAs technology

InGaAs/GaAs/InP heterostructures have been intensively investigated for long-wave electronic and optoelectronic applications such as: EDFA fiber amplifiers, light sources and photodetectors operating at 1300 nm and 1500 nm [1,2]. Recently strained InGaAs/AlGaAs/GaAs heterostructures have received considerable attention. The addition of Al to InGaAs alloys shifts the band gapt o higher energies, what makes them very attractive for device application in the visible part of the spectrum. Diode lasers working at 808 nm and in the range of $650 \div 730$ nm have been widely used for Nd:YAG pumping, drug activation and printing, respectively. In the work the studies of MOVPE growth of InAlGaAs / AlGaAs / GaAs heterostructures are presented. The composition of InAlGaAs quaternary alloy and its structural properties were investigated.

The following test structures were obtained:

I. semi-insulated GaAs (100) substrate — 500 nm GaAs buffer layer — MQW region consisted of $3\times$ $In_xAl_yGa_{1-x-y}As$ / GaAs — 70 nm GaAs cap layer,

II. semi-insulated GaAs (100) substrate — 500 nm GaAs buffer layer — MQW region consisted of $3\times$ $In_xAl_yGa_{1-x-y}As$ / $Al_zGa_{1-z}As$ — 70 nm GaAs capla yer,

III. semi-insulated GaAs (100) substrate — 500 nm GaAs buffer layer — MQW region consisted of $3\times$ $In_xAl_yGa_{1-x-y}As$ / $Al_zGa_{1-z}As$.

The growth temperature (T_g) was in the range of $650 \div 670$°C, the H_2 flow rate through TMIn bubbler ($V_{H2/TMIn}$) was varied from 35 to 75 ml/min. The other growth parameters were the same as for the InGaAs / GaAs MQW structures [3, 4].

* e-mail: Marek.Tlaczala@pwr.wroc.pl

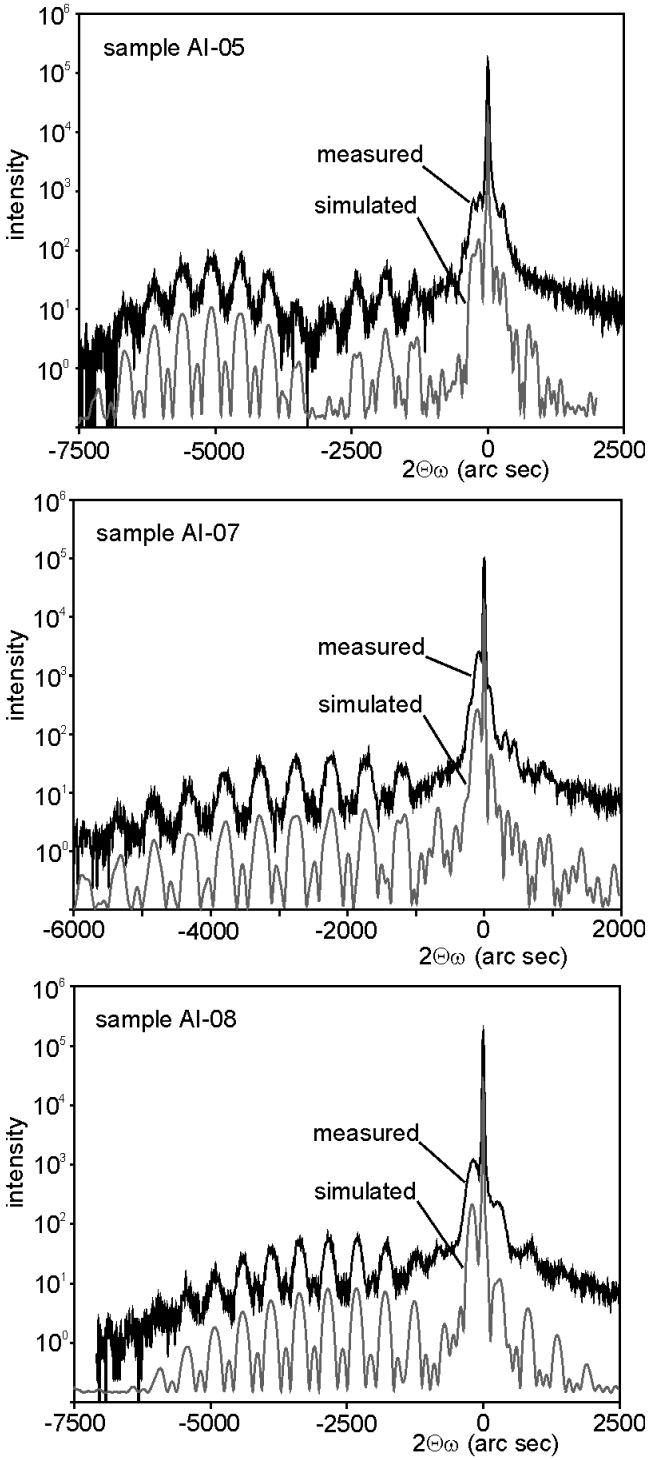

Fig. 1. Diffraction profiles of MQW structures: a) $In_{0.29}Al_{0.32}Ga_{0.39}As/GaAs$, b) $In_{0.20}Al_{0.29}Ga_{0.51}As/GaAs$, c) $In_{0.20}Al_{0.25}Ga_{0.55}As/Al_{0.45}Ga_{0.55}As$

The structural properties of the obtained structures were examined using HRXRD. Figure 1 shows the diffraction profiles of the test structure type I (Fig. 1a, sample AI-05), the test structure type II (Fig. 1b, sample AI-07) and the test structure type III (Fig. 1c, sample AI-08). The temperature of preparing sample AI-05 was 650°C and the InAs content was the highest (29%). In the samples fabricated at the temperature 670°C InAs content was 20% with the same H_2 flow rate through the TMIn bubbler. The thickness fringes observed in the measured profile indicate a perfect quality of the MQW region interfaces.

The composition profiles obtained for the test structures type I and type II by SIMS technique (Fig. 2), indicate high quality of the MQW region (uniformity of the thickness and composition), which confirms results obtained by HRXRD.

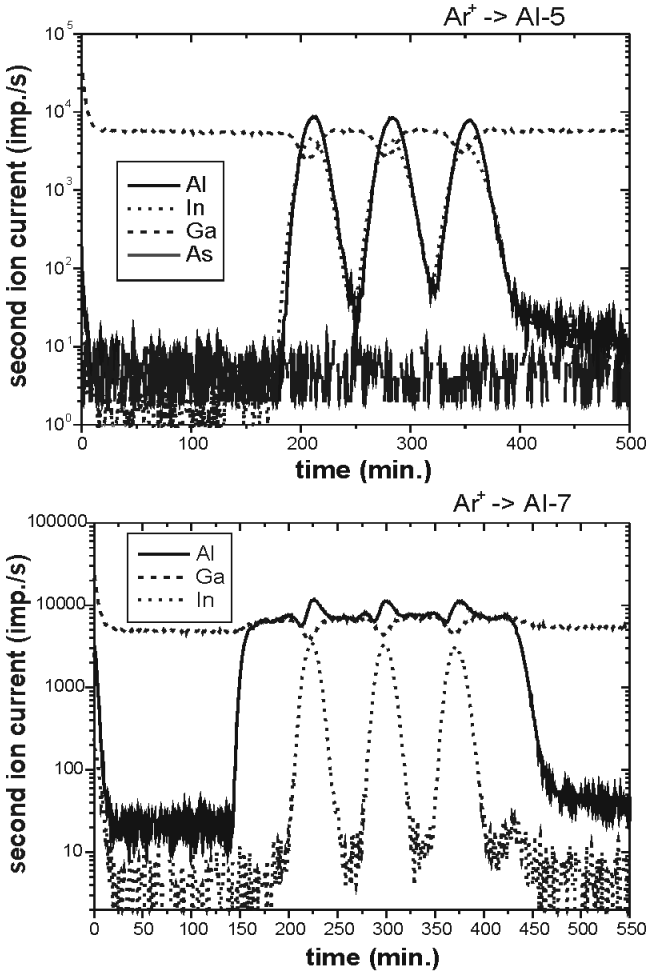

Fig. 2. The composition profiles obtained by SIMS technique: a) type I and b) type II test structure

Higher values of InAs content in the InAlGaAs quaternary alloy were achieved for lower growth temperatures. Applied technology allowed us to obtain high quality InGaAs/AlGaAs/GaAs MQW heterostructures.

3. Delta-doping of AIII-BV semiconductor compounds

Elaboration of semiconductor nanostructures technology requires clever and controlled manipulation of both material composition and doping process. Delta-doping (δ-doping, planar-doping) is a novel doping method of

semiconductors, which allows one to limit a doping region to a single or a few atomic layers. In this case dopant distribution can be described by Dirac-delta function [5, 6]:

$$n(z) = n_{2d}\delta(z - z_d) \tag{1}$$

where, n_{2d} is the two-dimensional doping density, z_d is the location of the doping plane.

Delta-doping, especially important for application in low dimensional structures (LDS), is mainly realised by two epitaxial methods: molecular beam epitaxy (MBE) and metalorganic vapour phase epitaxy (MOVPE). This kind of doping technique modifies the electronic structure of doped semiconductors by bending the conduction or valence band edges to form V-shaped (n-type doping) or inverted V-shaped (p-type doping) potential well. The ground state wave function is considerably delocalised (z_0 parameter) in the growth direction and can be calculated from the following equation [5]:

$$z_0 = 2\sqrt{\frac{7}{5}}\left(\frac{4}{9}\frac{\varepsilon\hbar^2}{e^2 n_{2d} m^*}\right)^{1/3} \tag{2}$$

where, ε is the semiconductor permittivity, e the elementary charge, m^* the effective mass. Structures with n-type and p-type delta doped layers are called "sawtooth superlattices". Delta-doping is widely applied in advanced electronic and optoelectronic devices, such as: high electron mobility transistor HEMT, heterojunction bipolar transistor HBT, resonant tunnelling diodes (RTDs), quantum well infrared photodetectors (QWIP), modulators and lasers.

The investigations of Si (n-type), Zn (p-type) δ-doped GaAs epilayers and centre Si-δ-doped $In_xGa_{1-x}As$ single quantum well (SQW) are presented. The δ-doping layer was formed by SiH_4 or DEZn introduction during the growth interruption. A basic δ-doping procedure was applied including pre-δ-doping purge, δ-doping, and post-δ-doping purge steps [5-7]. The electrical and optical properties of the obtained structures were examined using:

- C–V mercury probe with a HP 4192A impedance analyser (5 Hz÷13 MHz), PN4300 Bio-Rad EC–V electrochemical profiler and Raman spectroscopy (RS) — dopant concentration and broadening,
- photoreflectance (PR) and photocurrent (PC) spectroscopies — optical transitions.

The C–V profiles of Si-δ-doped GaAs and Zn-δ-doped GaAs epilayers are presented in Fig. 3 and Fig. 4.

Symmetric, Gaussian-function like doping C–V profiles were obtained for Si-δ-doped GaAs. The best C–V profile has a width of 5.5 nm (comparable with the spatial extent of the ground-state electron wave function z0) with corresponding sheet carrier concentration of 3×10^{12} cm^{-2}. The EC–V profiles of Zn-δ-doped GaAs exhibit symmetric and asymmetric Dirac δ-function like distribution. To achieve high hole concentration the post-δ-doping purge step was not applied. The best hole profile has a peak density of 8.8×10^{18} cm^{-3} with a broadening of 8.2 nm and the corresponding sheet hole density of 1.5×10^{13} cm-2. The best carrier confinement was achieved by introducing δ-doping into $In_xGa_{1-x}As$ QW. Dependence of the Si dopant concentration and its broadening ($FWHM_{C--V}$) in δ-doped region on $In_{0.22}Ga_{0.78}As$ quantum well widths is shown in Fig. 5a, b. The symmetric C–V profile with a carrier confinement of 2.8 nm and high sheet carrier density of 3.3×10^{12} cm^{-2} was obtained for QW width $L_w = 10$ nm.

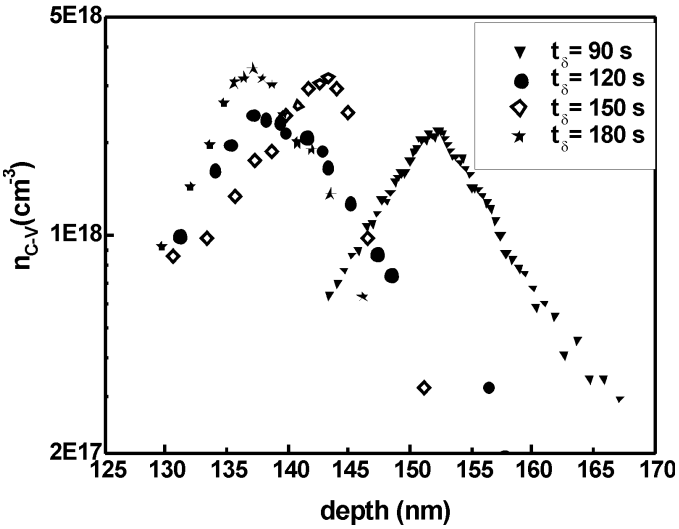

Fig. 3. The C–V profiles of Si-δ-doped GaAs obtained for different delta doping time t_δ

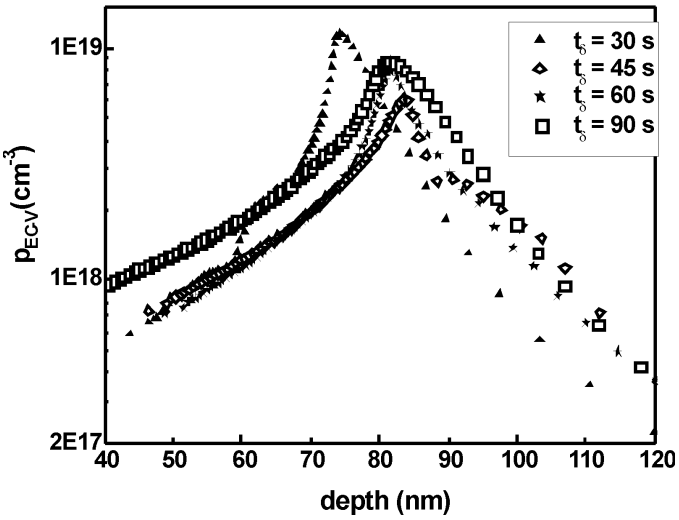

Fig. 4. The EC–V profiles of Zn-δ-doped GaAs obtained for different delta doping time t_δ

The results of C–V and EC–V measurements obtained for different δ-doped structures are listed in Table 1.

Table 1
The results of C–V and EC–V measurements

structurem	z_d [nm]	$n(p)_{C-V(EC-V)}$ [cm^{-3}]	$n(p)_{2d}$ [cm^{-2}]	$FWHM_{C-V(EC-V)}$ [nm]
Si-δ-doped GaAs	152	2.1×10^{18}	3.0×10^{12}	5.5
Zn-δ-doped GaAs	81	8.8×10^{18}	1.5×10^{13}	8.2
Si-δ-doped $In_xGa_{1-x}As$ QW ($x = 0.08$)	146	6.2×10^{18}	3.7×10^{12}	4.3
Si-δ-doped $In_xGa_{1-x}As$ QW ($x = 0.22$)	143	1.0×10^{19}	3.3×10^{12}	2.8

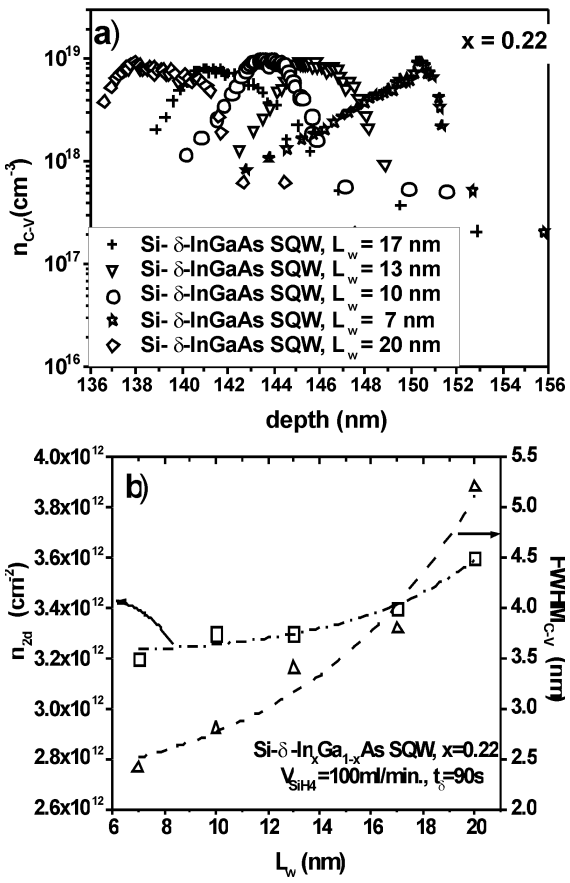

Fig. 5. Influence of Si-δ-doped In0.22Ga0.78As quantum well width on: a) C–V doping profiles, b) sheet carrier density and value of $FWHM_{C-V}$

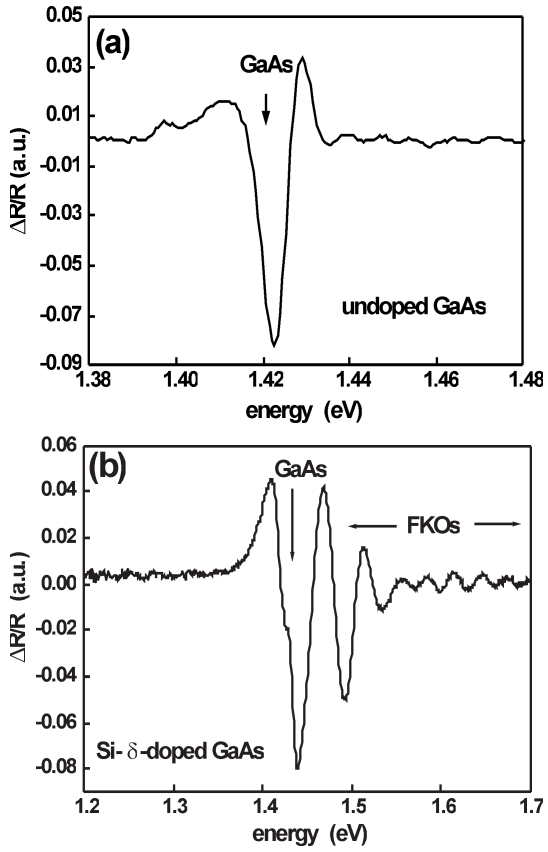

Fig. 6. The PR spectra of: a) undoped GaAs, b) Si-δ-doped GaAs

Optical properties Si-δ-doped structures were examined using PR and PC spectroscopy. The PR spectra of Si-δ-doped GaAs and Si-δ-doped $In_xGa_{1-x}As$ QW are presented in Fig. 6a, b and Fig. 7a, b, c. The undoped structures were used as the reference samples (Fig. 6a, 7a). In the case of Si-δ-doped GaAs (Fig. 6b) a lot of distinguished Franz-Keldysh oscillations (FKOs) above the band gapen ergy are seen, demonstrating the existence of a strong uniform electric field ($\sim$ 44 kV/cm) introduced by Si-δ-layer. For undoped $In_xGa_{1-x}As$ QW a lot of optical transitions inside QW are visible in PR spectrum (Fig. 7a), indicating high quality of the obtained structure.

In the case of Si-δ-doped $In_xGa_{1-x}As$ QW, due to the filling of the first electron subband, a transition involving this level is impossible. The 11H transition between the first heavy hole and first electron subband disappears, and only transitions involving higher electron subbands are observed in PR spectrum (Fig. 7b). For higher dopant concentrations (Fig. 7c), the optical transitions inside QW are not visible due to the occupation of all electron subbands by carriers. Calculated value of the internal electric field ($\sim$ 40 kV/cm), estimated from FKOs, is nearly the same as for Si-δ-doped GaAs.

Photocurrent (PC) measurements were realized on Au-Schottky photodiodes using standard lock-in technique and halogen source. The PC spectra of undoped and Si-δ-doped $In_xGa_{1-x}As$ QW are presented in Fig. 8a, b.

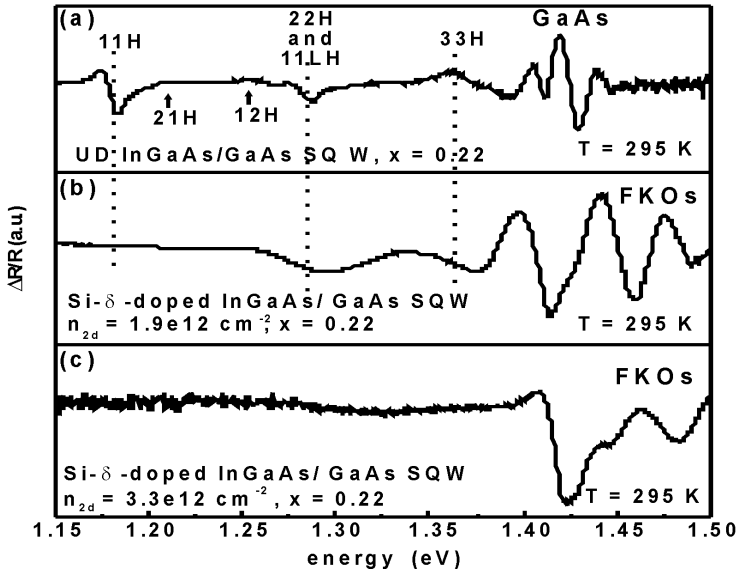

Fig. 7. The PR spectra of: a) undoped $In_{0.22}Ga_{0.78}As$ QW, b) Si-δ-doped $In_{0.22}Ga_{0.78}As$ QW ($L_w = 10$ nm, $n_{2d} = 1.9 \times 10^{12}$ cm^{-2}), c) Si-δ-doped $In_{0.22}Ga_{0.78}As$ QW ($L_w = 10$ nm, $n_{2d} = 3.3 \times 10^{12}$ cm^{-2})

Obtained spectra are influenced by an electrical field introduced by δ-doped layer (FKOs oscillation above the band gap energy of GaAs). The PC spectrum of undoped $In_xGa_{1-x}As$ QW shows two peaks below GaAs absorption edge, corresponding to 11 H and 11 LH absorption in $In_xGa_{1-x}As$ QW (Fig. 8a).

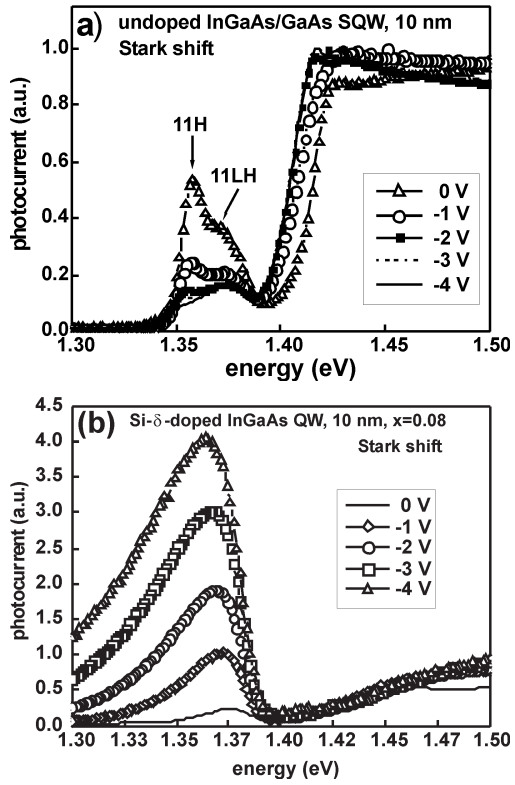

Fig. 8. Photocurrent response of: a) undoped $In_xGa_{1-x}As$ QW, b) Si-δ-doped $In_xGa_{1-x}As$ QW ($L_w = 10$ nm, $x = 0.08$), at different reverse bias voltage

The PC signal related to the 11H transition decreases and shifts the position (about — 1.5 meV/V) by changing the reverse bias voltage due to the lowering of the probability of these optical transitions and Quantum Confined Stark Effect (QCSE). In the case of PC spectrum of Si-δ-doped $In_xGa_{1-x}As$ QW only one maximum below GaAs absorption edge is observed, corresponding probably to 12LH or 22H absorption in the QW, because of "band filling effect" (Fig. 8b). In contrast to the undoped QW, this maximum increases and considerably shifts position (about — 4 meV/V) under reverse bias voltage in effect of increased escape of photogenerated carriers and enhanced QCSE [8, 9].

Introducing delta-doping into QW gives a better carrier confining. In addition, the results of PR and PC measurements showed significant modification of optical transitions of Si-δ-doped InGaAs/GaAs SQW structures.

4. AIII-N structures

Possibility of application of AIII-N heterostructures depends both on fabrication of high quality substrates GaN and possibility of precise control of growth and Mg-doping processes.

4.1. From thick GaN layers to freestanding substrates. In the nature there are no native crystals of the gallium nitride, their synthesis is very difficult and single crystals with good properties are hardly available. Crystallisation of freestanding GaN substrates can be carried out by either high-pressure synthesis [10], by sublimation method [11] or ammonothermal method [12]. However, the size of GaN crystals obtained in these methods is still too small for practical use. Currently, the largest freestanding GaN substrates are obtained by growing a thick

GaN layer on a sapphire substrates using Hydride Vapour Phase Epitaxy (HVPE) and separating the grown layers from the sapphire. It is the reason of the use of alternative substrates in AIII-N technology.

The use of the alternative substrates for nitrides epitaxy causes generation of numerous misfit dislocations because mismatch of lattice parameters and coefficients of thermal expansion are high (Fig. 9) [13]. The fundamental problem is the choice of the alternative substrate, nucleation layer and method to separate deposited GaN epilayers from the substrate. However, at present, this is the only practical way to obtain thick GaN layers with a good quality that can be applied to manufacturing freestanding substrates for epitaxial growth of the device structures.

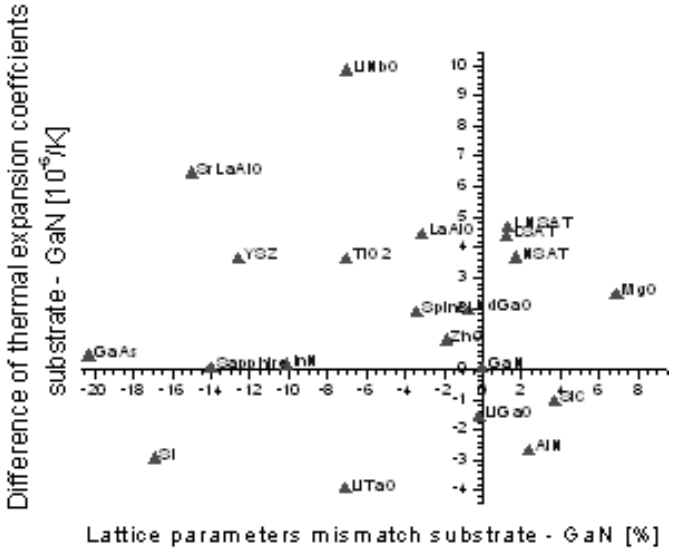

Fig. 9. Mismatch oflat tice parameters and thermal expansion coefficients: alternative substrates — GaN

In our experiments thick GaN layers were grown in conventional, open HVPE system: three-temperature zone furnace and horizontal quartz reactor, described in detail elsewhere [14, 15]. Nitrogen (6N) was used as the carrier gas. GaCl was formed by the reaction of gaseous HCl (6N) and liquid Ga (6N) at 920°C. HCl was diluted by nitrogen. NH3 (7N) was used as the source gas. Total gas flow rate was about 4500 ml/min. The temperature in the growth zone was kept at 1054°C.

The samples were grown directly on the sapphire substrates by the three-steps technique. The Al_2O_3substrate was preheated in ambient nitrogen and ammonia at 1054°C, and then nucleation layer was deposited at 600°C with a small amount of GaCl. Then, the sample was transferred to the high temperature zone to enable migration and collapse of GaN islands — GaN crystal nuclei. Then, the growth was continued — (a) low rate growth step — about 6 μm/h and (b) high rate growth part — more than 25 μm/h.

In our investigations we made thick GaN layers up to 100 microns and the sizes of crystalline blocks are to 2000 nm [14]. Images of the sample, cross-section of thick GaN layer and topvi ew of GaN substrate are presented in Fig. 10.

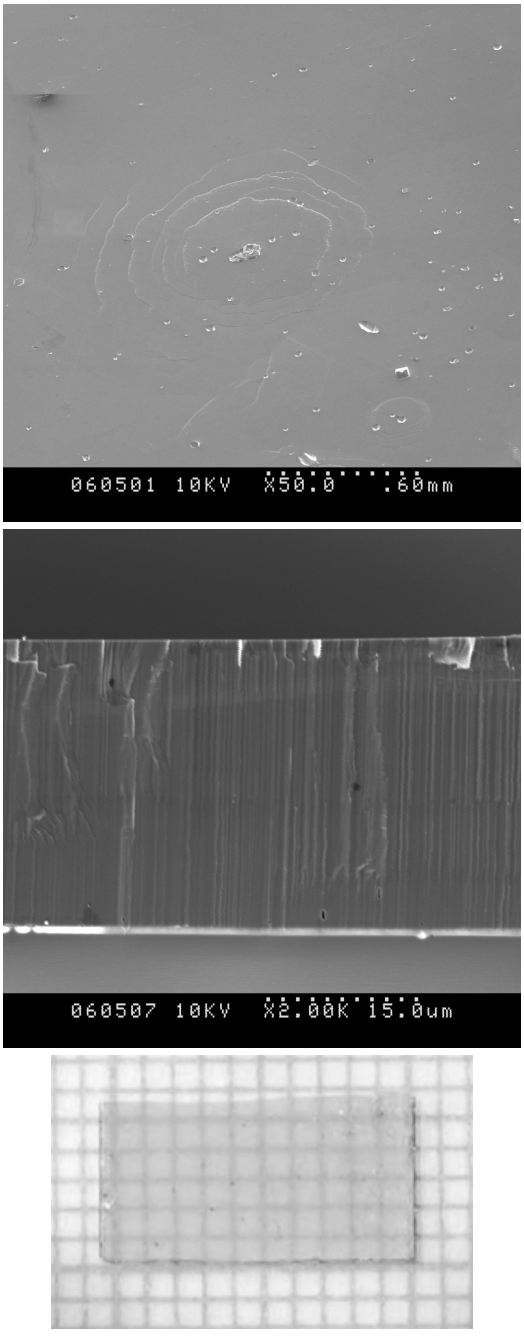

Fig. 10. Images of sample G3: (a) grown surface from SEM, (b) cross-section from SEM, (c) view from digital camera

Technology of thick GaN layers grown on sapphire by HVPE is very promising as a part of freestanding GaN substrates manufacturing. Further works will be focused on optimisation of growth, separating layers from substrates and surface polishing.

4.2. The growth of *p*-type GaN layers. The growth of highly conductive *p*-type GaN is an essential part of the fabrication of optoelectronic devices. To date, Mg is the only known acceptor in GaN that reliably generates a hole conduction. Typical values of the free hole concentration at room temperature (RT) are in the 10^{17}–10^{18} cm^{-3} range. The high Mg acceptor binding energy and compensation effects, observed in the highly doped layers, are the main reasons why higher values for the free hole concentration is difficult to achieve. In the case of GaN:Mg layers grown by metalorganic vapour phase epitaxy (MOVPE), the additional effect of hydrogen has to be considered because the formation of electrically inactive acceptor-hydrogen complexes was observed when ammonia (NH3) was used as the nitrogen source. These Mg-H complexes are responsible for high resistivity of as-grown layers [16]. The high temperature thermal annealing of GaN:Mg layers must be performed to dissociate these complexes and thus electrically activate the acceptor dopant. It was shown that the kinetics of activation process depends on the temperature and atmosphere in the annealing environment but electrical characteristics of GaN:Mg layers are, still not well understood [17].

The ~ 1.5 μm thick Mg-doped GaN layers (sample $1 \div 4$) used in this study were grown in a horizontal MOVPE reactor, on (0001) sapphire substrates, using trimethyl gallium (TMGa), bis-cyclopentadienyl magnesium (Cp_2Mg) and ammonia. The GaN (sample 1, 2, 3) or AlN (sample 4) low temperature layers were applied as a nucleation layer (Fig. 11). In this study all layers were prepared under exactly the same growth conditions except the dopant concentration in the reactor and the temperature during the growth. If we assume that the flow of Cp_2Mg during the growth of sample 1 and sample 4 was unity, then the respective flow during the growth of sample 2 was twice as high and three times higher for sample 3. The GaN:Mg layers were grown at 1050°C (sample 1,2,3) while sample 4 was grown at 1200°C. The incorporation of Mg was verified by SIMS (Table 2). The as grown GaN:Mg layers resistivity were as follows: $\sim 0.83\Omega\cdot$ cm (sample 1), $\sim 0.4\Omega\cdot$ cm (sample 2), $\sim 3.0\Omega\cdot$ cm (sample 3), $\sim 7.8\Omega\cdot$ cm (sample 4). Then, each sample was cut into pieces and furnace annealed in pure N_2 ($800 \div 850$°C, 30 min.) or O_2 ($500 \div 550$°C, 30 min.). Such conditions were suggested, in the literature, as the optimal condition of the acceptor dopant activation in GaN:Mg layers.

Non destructive method was used to sample characterisation. To clarify the influence of activation process parameters on the GaN:Mg layer properties we applied low temperature photoluminescence (PL) measurements and impedance spectroscopy method.

The PL spectra of as grown and annealed layers were studied. Mg-related emission at ~ 3.2 eV was observed. The relative intensity between bandgap- and Mg-related emissions changes with the increase in Mg concentration in favuor of Mg-related emission. The annealing process enhances PL intensity without significant change in the shape of PL spectrum. It was observed that all annealed samples showed much stronger blue emission and weaker deep-level emission compared to as grown samples. The samples $1 \div 3$ annealed in pure O_2 have shown a stronger blue emission and weaker deep-level emission compared to samples annealed in pure N_2, while sample 4 annealed in pure N_2 showed stronger blue emission than the sample annealed in pure O_2 (Table 2). It confirms that some non-radiative centers, which probably are related to Mg atoms, can be removed by the post-growth annealing.

Table 2
Optical and electrical characteristic of the samples $S1 \div S4$ (YB — yellow band, BB — blue band)

Sample	Mg (SIMS) [cm^{-3}]	Annealing	ρ [$\Omega\cdot$ cm]	τ [μsec]	N_a–N_d [cm^{-3}]	PL Intensity [a.u.]	
						BB	YB
S1 (on LT-GaN)	$2*10^{18}$	as-grown	0.83	2700	?	2435	6000
		N_2, 800°C, 30 min	0.49	20.4	$1\cdot10^{18}$	2201	421
		O_2, 500°C, 30 min	0.41	?	?	4808	1000
S2 (on LT-GaN)	$4*10^{18}$	as-grown	0.4	49.4	$5.5\cdot10^{17}$	3972	300
		N_2, 800°C, 30 min	0.36	5.1	$6.5\cdot10^{18}$	6980	60
		O_2, 500°C, 30 min	0.38	36.7	$5.5\cdot10^{18}$	9852	300
S3 (on LT-GaN)	$1*10^{19}$	as-grown	3.0	45.5	$1\cdot10^{18}$	11092	350
		N_2, 800°C, 30 min	1.1	3.7	$1.3\cdot10^{19}$	4401	50
		O_2, 500°C, 30 min	2.6	41.1	$9\cdot10^{17}$	13475	200
S4 (on LT-AlN)	$2*10^{18}$	as-grown	7.8	29.6	$7\cdot10^{17}$	4194	50
		N_2, 800°C, 30 min	3.5	2.5	$2.5\cdot10^{18}$	7792	50
		O_2, 500°C, 30 min	7.2	24.2	$7\cdot10^{17}$	4906	50

The electrical properties of the epitaxial layers were determined by the C–V measurements performed in a range of frequencies (80 Hz ÷ 10 MHz), using HP 4192A Impedance Meter equipped with a two column mercury probe. The details of the measurement procedure were discussed previously [18] (Table 2). The C and G versus frequency characteristics of GaN:Mg layers were measured in the range of dc biases and the results were fitted to the worked-out model. The example of capacitance and conductance spectra, obtained for sample S3, are shown in Fig. 11. Spectra from the other samples have a similar shape. The layers parameters variation with the annealing process condition was evaluated. The strong dependence of capacitance spectra vs. frequency was observed. The values of capacitance at low and high frequencies differ significantly from each other. It means that almost all acceptors in GaN:Mg layers were trapped at room temperature. The net (N_a-N_d) carrier concentration as a function of the distance from the top surface was calculated from the changes of capacitance versus bias characteristics, obtained at low frequency. The obtained concentration was the sum of free and trapped holes.

The impedance spectroscopy method allowed us also to determine GaN:Mg layers resistivity [19]. It was observed that Mg activation depends not only on the Mg concentration in the as-grown GaN:Mg layers but is also affected by their structure. Samples S1 and S4, which differ from each other only by the nucleation layers and the growth temperature, had the same magnesium concentration, determined by SIMS. After N2 annealing at 800°C for 30 min. the net carrier concentrations in both samples were the same while the resistivity of sample S4 was almost ten times grater than that of sample S1.

The intensity of the blue band of the PL spectra was not correlated with electrical parameters of the layers. It was stated that the high magnesium concentration in as-grown layers (sample S3) led to high intensity of the blue band of PL spectra.

There was an optimal concentration of magnesium in as-grown GaN:Mg layer (sample S2). It allowed us to obtain the lowest value of layer resistivity. This value did not depend on the annealing process. Formally, it means that in non annealed samples (S2) the higher mobility was observed (~ 15 cm^2/V·s). For all remaining samples this value was not higher than about 1 cm^2/V·s.

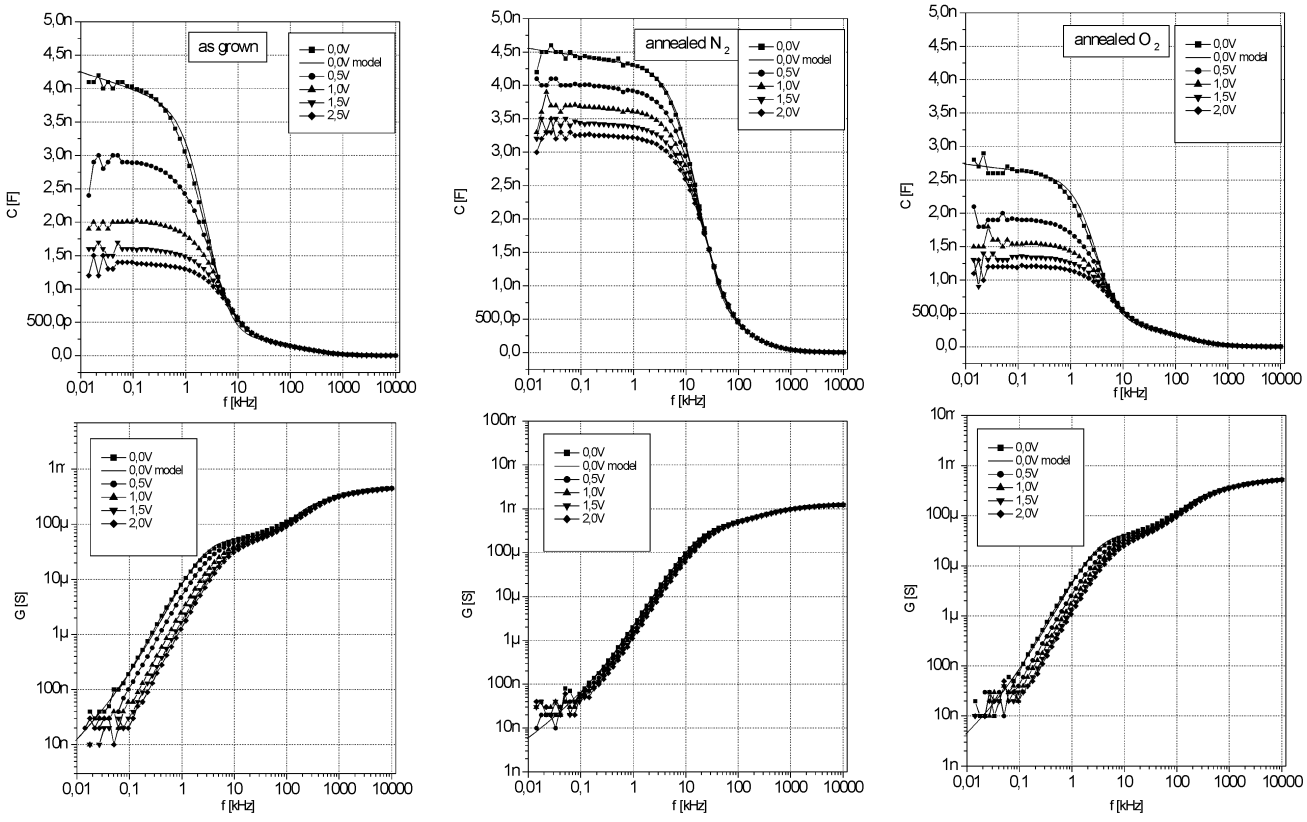

Fig. 11. The capacitance and conductance vs. frequency for mercury contact to S3 sample (dots denote measured results, solid line represents simulation result). From left to right: as-grown, N_2 annealed and O_2 annealed

It was stated that the annealing process affected mainly the net carrier concentration of the samples and relaxation time of the traps (their activation energy). The O_2 annealing at 500°C for 30 min., did not affect the relaxation time of the traps although that parameter decreased significantly after N2 annealing at 800°C for 30 min. For the optimal doping condition (sample S2) the net carrier concentration approached its almost maximum value just after O_2 annealing at 500°C. The effect was not observed for samples S3 and S4 which must have been annealed at N_2 800°C to obtain maximum value of the net carrier concentration. The net carrier concentration of all samples depended not only on the magnesium concentration in as-grown GaN:Mg layer.

It was observed that for samples S3 and S4 the change in net carrier concentration vs. annealing process parameters was similar in spite of the fact that the magnesium content in as-grown layer (verify by SIMS) was different.

Good correlation was observed between the relaxation time of the trapa nd the intensity of yellow band of the PL spectra (Table 2). It was not affected by the annealing process. For Sample S4 the yellow band wasn't observed.

The PL spectra of sample S4, without YB, may suggest that it has improved crystalline structure. This sample has also the highest resistivity. The high resistivity with the similar value of net carrier concentration may be interpreted as the low mobility of the holes. This unexpected behaviour needs further studies.

5. Conclusion

Elaborated technology of AIII-BV and AIII-N semiconductor compounds allowed us to obtain high quality epitaxial heterostructures with precise control of composition and doping for application in advanced device structures.

Acknowledgements. The authors would like to thank prof. J. Kováč from Slovak University of Technology and prof. J. Misiewicz from Wrocław University of Technology for PC and PR measurements. This work was partially supported by Wroclaw University of Technology Advanced Materials and Nonotechnology Centre, Polish Science Foundation (Project TECHNO 106/2000, TECHNE 6/2001), Polish State Committee for Scientific Research under Grants 4 T11B 061 24, 4 T11B 012 23, 4 T11B 035 25 and Wroclaw University of Technology statutory grant.

References

[1] P. J. A. Thijs, at al., *J. Cryst. Growth* 93, 863 (1988).

[2] E. Desurvire, *Erbium-dopped Fiber Amplifiers: Principles and Applications*, John Wiley and Sons, New York, 1994.

[3] M. Tłaczała, J. Kozłowski, D. Radziewicz and R. Korbutowicz, *Heterostructure Epitaxy and Devices-HEAD'97*, Kluwer Academic Publishers, 119 (1998).

[4] D. Radziewicz, at al., *Mol. Phys. Report* 21, 113 (1998).

[5] G. Li and C. Jagadish, "Recent progress in δ-doping of III-V semiconductors grown by metal organic vapour phase epitax", *Solid-State Electronics* 41, 1207 (1997).

[6] E. F. Schubert, "Delta doping of III-V compound semiconductors: Fundamentals and device applications", *J. Vac. Sci. Technol. A* 8, 2980 (1990).

[7] B. Ściana, D. Radziewicz, B. Paszkiewicz, M. Tłaczała, M. Utko, P. Sitarek, G. Sęk, J. Misiewicz, R. Kinder, J. Kováč and R. Srnanek, "MOVPE technology and characterisation of silicon δ-doped GaAs and $Al_xGa_{1-x}As$", *Thin Solids Films* 412, 55–59 (2002).

[8] Tang Xiaohong and Chua Soo Jin, "Saturation of the nonlinear absorption in n-i-p-i multiple quantum well structures", *Mater. Sci. Eng.* B35, 72 (1995).

[9] N. Linder, T. Gabler, H. Gulden, P. Kiesel, M. Kneissl, P. Riel, G. H. Döhler, X. Wu, J. Walker and J. S. Smith, "High contrast electro-optic n-i-p-i doping superlattice modultor", *Appl. Phys. Lett.* 62(16), 1916 (1993).

[10] S. Porowski, "Growth and properties of single crystalline GaN substrates and homoepitaxial layers", *Mater. Sci. Eng.* B44, 407 (1997).

[11] P. G. Baranov, E. N. Mokhov, A. O. Ostroumov, M. G. Ramm, M. S. Ramm, V. V. Ratnikov, A. D. Roenkov, Yu. A. Vodakov, A. A. Wolfson, G. V. Saparin, S. Yu. Karpov, D. V. Zimina, Yu. N. Makarov and H. Juergensen, "Current status of GaN crystal growth by sublimation sandwich technique", *MRS Internet J. Nitride Semicond. Res.* 3, 50 (1998).

[12] R. Dwiliński, R. Doradziński, J. Garczyński, L. Sierzputowski, M. Palczewska, A. Wysmołek and M. Kamińska, "AMMONO method of BN, AlN and GaN synthesis and crystal growth", *MRS Internet J. Nitride Semicond. Res.* 3, 25 (1998).

[13] R. Korbutowicz, E. Dumiszewska and J. Grabowska, "Podłoża alternatywne stosowane w epitaksji azotku galu", *Elektronika* 11, 1 (2003), (in Polish).

[14] R. Korbutowicz, J. Kozłowski, E. Dumiszewska, J. Serafińczuk, "X-Ray characterization of thick GaN layers grown by HVPE", *Crystal Res. & Technol.*, (to be published).

[15] R. Korbutowicz, "Thick GaN layers grown by HVPE", *Applied Physics of Condensed Matter*, pp. 130–133 (June 16–18, 2004).

[16] W. Gotz, M. Johnson, D. P. Bour, "Deep level defects in Mg-doped, *p*-type GaN grown by metalorganic chemical vapor deposition", *Appl. Phys. Lett.* 68, 3470 (1996).

[17] S. J. Chang, Y. K. Su, T. L. Tsai, C. Y. Chang, C. L. Chiang, C. S. Chang, T. P. Chen, K. H. Huang, "Acceptor activation of Mg-doped GaN by microwave treatment", *J. Electron. Mat.* 32, 395 (2003).

[18] B. Paszkiewicz, "Impedance spectroscopy analysis of AlG aNGaN HFET structures", *J. Cryst. Growth* 230, 590 (2001).

[19] J. R. MacDonald, *Impedance Spectroscopy*, John Wiley & Sons, New Jork, 1987.